Physical properties of Sm_xB_6 single crystals

Jolanta Stankiewicz,[1] Marco Evangelisti,[2] Priscila F. S. Rosa,[3] Pedro Schlottmann,[4] and Zachary Fisk[5]
[1]*Departamento de Física de la Materia Condensada, Universidad de Zaragoza, 50009 Zaragoza, Spain*
[2]*Instituto de Ciencia de Materiales de Aragón and Departamento de Física de la Materia Condensada, CSIC–Universidad de Zaragoza, 50009 Zaragoza, Spain*
[3]*Los Alamos National Laboratory, Los Alamos, New Mexico 87545, USA*
[4]*Department of Physics, Florida State University, Tallahassee, Florida 32306, USA*
[5]*Department of Physics and Astronomy, University of California, Irvine, California 92697, USA*

(Received 27 October 2018; published 24 January 2019)

We study the magnetic susceptibility, electrical resistivity, Hall effect, and heat capacity of single crystals of Sm_xB_6 for $x = 1, 0.94, 0.8,$ and 0.75. Remarkably, the overall properties of the crystals do not qualitatively depend on the density of vacancies. The topological surface states are seen at low temperatures in the electrical transport properties as the bulk conductivity freezes out. Even a large number of Sm vacancies does not close the hybridization gap. The linear term in the specific heat γ, of unclear origin, remains large but decreases gradually with x. The shoulder in the density of states, brought by the hybridized $4f$ states and observed in the susceptibility and the specific heat, does not move but decreases its height with decreasing x. The specific heat also displays a weak Schottky anomaly at about 1.5 K for all x, except for the $x = 0.75$ sample. This Schottky anomaly is only slightly field dependent and of unknown origin.

DOI: 10.1103/PhysRevB.99.045138

I. INTRODUCTION

Many divalent hexaboride compounds, either with a rare-earth metal (Sm or Eu) or alkaline-earth metal (Ca, Sr, or Ba), show intriguing physical behavior at low temperatures despite their rather simple cubic CsCl-type crystal structure, in part due to the presence of a certain amount of native defects, usually ascribed to boron or cation vacancies. This disorder is enhanced since the cation is weakly bound at the center of an oversized "cage" consisting of 48 boron atoms and can be displaced easily from its equilibrium position. The boron framework, on the other hand, is rigid, leading to high melting points and low coefficients of thermal expansion. All this makes for extraordinary behavior observed in these compounds. Samarium hexaboride, SmB_6, is a mixed-valent semiconductor, where the Sm ions are present as both Sm^{2+} ($4f^6$) and Sm^{3+} ($4f^5 5d$), with all the Sm sites being crystallographically equivalent.

Early experimental and theoretical work established SmB_6 as a Kondo insulator [1–4]. The high-temperature correlated metallic behavior in this compound changes to an insulating one below approximately 40 K due to the opening of energy gap $\Delta_K \approx$ 15–20 meV. This gap is brought about by the hybridization between the localized Sm $4f$ states and the weakly correlated, mainly Sm $5d$ states. A diverging resistance as the temperature tends to zero is expected for a Kondo insulator, but instead, the resistance flattens below approximately 5 K. The concept of a topological insulator (TI) [5], i.e., a material that has an insulating bulk with nontrivial topological protected surface states, was invoked as a plausible explanation for the low-temperature resistance saturation of SmB_6 [6–14].

Most of the recent experimental research on SmB_6 focused on its TI properties, conclusively showing that metallic surface conduction is the cause of the leveling off of the low-temperature resistivity. Among many other things, this research includes heat transport [15], angle-resolved photoemission spectroscopy (ARPES) [16–19], tunneling microscopy [20–23], neutron scattering [24], and novel electrical transport measurements [25–27]. Nevertheless, results of specific heat [28], optical conductivity [29], NMR relaxation [30], and quantum oscillation [31] measurements indicate a bulk origin of SmB_6 behavior at low temperatures. Currently, there is no physical picture that could explain all these results.

The role of defects and of the concomitant disorder in the properties of samarium hexaboride, despite being studied for several decades, remains an open question [32–35]. Systematic control of the stoichiometry for SmB_6 crystals is not easy. Rare-earth elements are difficult to purify, and samarium vaporization during growth, especially in a floating-zone technique, may give rise to compositional variations [35]. These factors, in addition to the tendency for disorder in hexaborides, might alter considerably the physical properties of SmB_6. On the other hand, control over doping would offer a direct way to relate low-temperature transport behavior to the bulk properties in this compound. Cation vacancies are of particular interest as they not only change carrier concentration but also may affect the Sm average valence. Therefore, studies of nonstoichiometric crystals could probe bulk properties of SmB_6 (in-gap states) and their impact on the topological aspects. So far published reports on the properties of nonstoichiometric SmB_6 contain contradictory results. Some reports claim a strong decrease of the resistivity on doping [33,36], which is not supported by other groups [37,38]. It is important to note that SmB_6 crystals studied in Refs. [33,36] were grown using the floating-zone method, whereas flux-grown crystals were used in Refs. [37,38]. Interestingly, Raman scattering

results suggest that 1% of Sm vacancies in any crystal can suppress the hybridization gap [39] and therefore modify significantly the properties of cation-deficient SmB_6. Thus, measurements on nonstoichiometric SmB_6 single crystals could contribute to our understanding of the physics behind the low-temperature behavior of this system.

In the present paper we study electrical transport, magnetic properties, and heat capacity of stoichiometric and nonstoichiometric SmB_6 single crystals in order to establish how disorder affects these properties. The remainder of the paper is as follows. The experimental procedure is described in Sec. II. Results of measurements are reported and discussed in Sec. III, and conclusions are drawn in Sec. IV.

II. EXPERIMENT

Single crystals of Sm_xB_6 were grown using an Al flux technique. Different starting compositions of Sm and B have been used to cover the x range from 0.6 to 1. We have used energy dispersive x-ray spectroscopy (EDS) to estimate the Sm content in the samples (see Supplemental Material) [40]. We find that the nominal concentration of vacancies in single crystals of Sm_xB_6 is close to the actual composition, except for the sample with the highest nominal amount of vacancies ($x = 0.6$). This is supported by our single-crystal x-ray diffraction measurements, which show that the lattice parameters of Sm_xB_6 crystals nearly saturate with decreasing x. In the following, we use the estimated EDS values of x.

We have measured at least two samples of each composition: an as-grown and a polished single crystal. In each case the samples were rinsed in $HCl:H_2O$ (1:10) for 60 s before measurements. Approximate dimensions of measured crystals along the cubic axes were $0.2 \times 0.4 \times 1.0$ mm^3. Contact leads (25- or 10-μm gold or platinum wire; see inset in Fig. 2 below) were spot-welded to the samples. Low-frequency transport measurements were carried out in helium cryostats with a six-probe method. The resistivity and Hall effect were measured as a function of magnetic field, from -2 up to 2 T, at all experimental points, from 0.34 up to 340 K. Hall resistivity varies linearly with magnetic field in the applied range. We have found that transport properties vary significantly with the preparation of the sample's surface, in agreement with previous studies. Details on this point are given in the Supplemental Material [40]. Here, we focus on results obtained for single-crystalline samples with no prior polishing.

The magnetization measurements in the temperature range from 2 to 340 K and in magnetic fields of up to 5 T were made using the same geometry as in electrical transport with a commercial superconducting quantum interference device (SQUID) magnetometer.

Our heat capacity measurements were performed in a Quantum Design physical properties measurement system (PPMS) with a ^{3}He insert in applied field of 0, 1, and 5 T. A small amount of Apiezon N grease, whose contribution to the heat capacity was subtracted *a posteriori*, was used to hold the crystal in place on a sapphire platform and to ensure good thermal contact between the crystal and the platform. The PPMS measures the heat capacity at high vacuum using the relaxation method. We used the same crystals in electrical transport, specific heat, and magnetic measurements. In this way, we expect to avoid composition uncertainty errors when comparing results of different experiments.

III. RESULTS AND DISCUSSION

The variation of the static magnetic susceptibility $\chi(T)$ with temperature for vacancy-doped SmB_6 crystals is shown in Fig. 1. These measurements were carried out at 1000 Oe. The susceptibility of all samples follows a dome-shaped curve centered at about 50 K, as already reported [41]. The maximum arises from the peak in the density of states above the hybridization gap and is well understood. The character changes below 15 K, where an upturn of $\chi(T)$ is observed, although naively one would expect a flat temperature-independent Van Vleck susceptibility due to transitions across the gap. In earlier days this low-temperature increase of $\chi(T)$ was attributed to the presence of paramagnetic impurities [42], and later it was attributed to in-gap magnetic excitonlike bound states [43–46]. These in-gap bound states correspond to the 16 meV peak observed in inelastic neutron scattering (INS) spectra [47]. They emerge at about $\sim$20 K, i.e., at a temperature much larger than 4 K, at which the low-T resistivity plateau arises, and are hence not related to the topological surface states. The temperature dependence of the intensity of the INS peak scales with the contribution of the in-gap state to the susceptibility [48,49] and with the intensity of the Raman transition [50].

To interpret quantitatively the $\chi(T)$ variation, contributions from the Sm^{2+} and Sm^{3+} ion configurations have to be

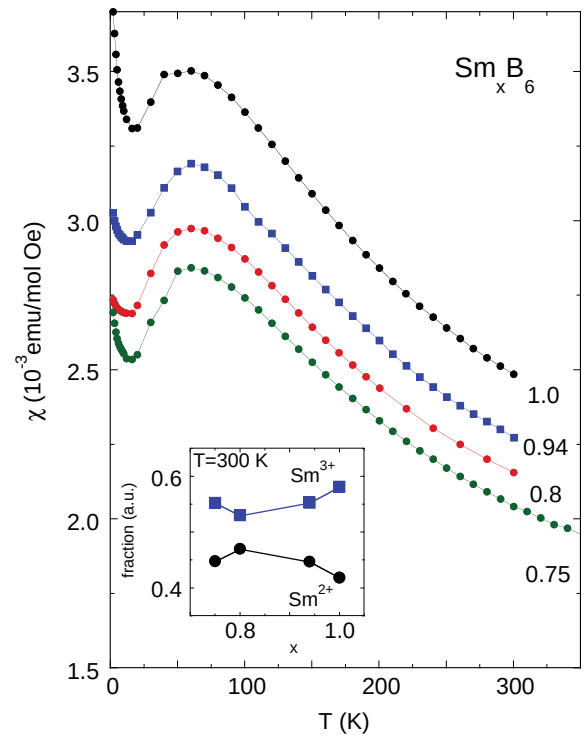

FIG. 1. Magnetic susceptibility vs T for Sm_xB_6 single crystals, measured using a SQUID magnetometer. In the inset we plot the fraction of Sm^{2+} and Sm^{3+} ions for crystals with different contents of vacancies.

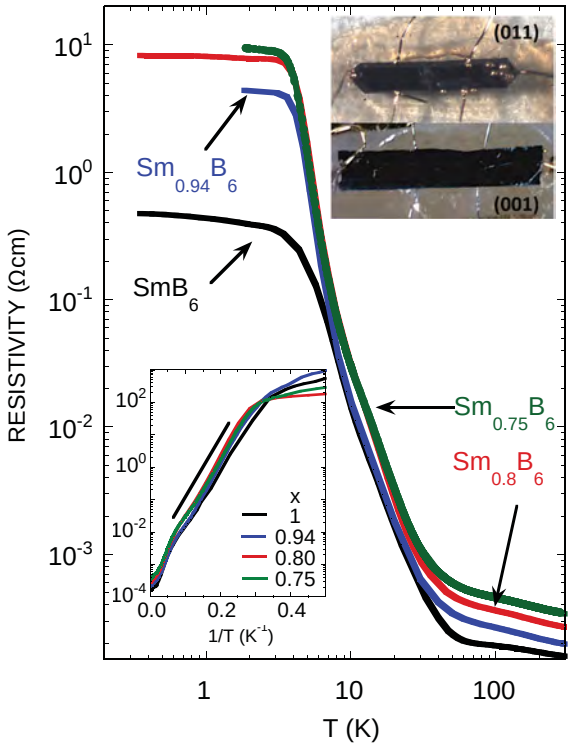

FIG. 2. Resistivity of Sm_xB_6 for as-grown single crystals vs temperature. The lower inset shows the bulk resistivity vs inverse temperature for the same crystals. The upper inset is the actual image of the transport geometry used in measurements.

taken into account. At low T the ground state is a quantum linear superposition of the two configurations, while at high T (e.g., room temperature) a description adding the contributions of the two states without interference works quite well. The inset in Fig. 1 shows the fractions of Sm^{2+} and Sm^{3+} ions in the crystals studied, estimated from the measured susceptibility at 300 K. The relative content of $Sm^{3+}(4f^5d^1)$ decreases slightly from 0.58 at $x = 1$ to 0.55 for $x = 0.75$. This is surprising since a Sm vacancy needs the $5d$ electrons of two Sm^{3+} ions to fill all the bonding orbitals. Thus, the limiting value of 3+ is expected for the Sm valency upon vacancy doping. On the other hand, this observation agrees with the electrical transport properties of the Sm_xB_6 system, discussed below, which show the resistivity increases and the carrier concentration decreases as the vacancy content becomes greater. Since the mixed-valence value stays nearly constant in Sm_xB_6 crystals, it fits the criteria for the formation of the low-temperature resistance plateau, as has been proposed from high-pressure studies on SmB_6 [51].

The temperature variation of the electrical resistivity in as-grown Sm_xB_6 single crystals is shown in Fig. 2. We found that the electronic transport properties are similar for all the Sm_xB_6 compounds we have studied. Previous studies of high-quality SmB_6 single crystals have shown the evolution of this system from a semimetallic state at room temperature to a Kondo-correlated insulating state and finally to a very low carrier density metallic state at low temperatures. It is now generally accepted that for $T \lesssim 5$ K, the transport in SmB_6 takes place through surface states (SS) as the bulk resistance R_b is much higher than the surface resistance R_s. With increasing temperature (4 K $\lesssim T \lesssim$ 10 K), R_b becomes comparable to that of the SSs, and the conduction proceeds through both the bulk of the crystal and the surface channels. Beyond 10 K and up to approximately 40 K, surface states are still seen in ARPES experiments, but the bulk resistance over this temperature range is much smaller than that of the surface states, and the latter have no effect on electrical transport. At temperatures higher than the Kondo temperature, electrical conduction is through the bulk with carriers (electrons and holes) arising from the X points of the Brillouin zone.

The resistivity of Sm_xB_6 shows similar behavior. It increases sharply at $T \approx 40$ K and, below $T \lesssim 5$ K, starts to level out. However, we do not observe a saturation of the resistivity down to 0.34 K, similar to the sample with $x = 1$. For $T > 40$ K, on the one hand, samarium vacancies introduce additional holes, increasing the conductivity, but on the other hand, they also generate scattering centers which decrease the conductivity due to the disruption of the coherence in the hybridization. The two competing effects yield an increase in the resistivity with x. To estimate the bulk resistivity, we use the relation $1/R = (1/R_b + 1/R_s)$, where R is the total resistance [27]. Assuming that the surface conductivity is independent of temperature and the simple geometry used (see the upper inset in Fig. 2), we obtain for the bulk resistivity values which are plotted in the lower inset of Fig. 2 as a function of the inverse temperature $1/T$. All samples show a thermally activated behavior $\rho_b \propto \exp(E_A/k_BT)$, with an almost identical activation energy of 3.9 meV (corresponding to the hybridization gap) from 30 down to 4 K. The bulk resistivity rises by more than 5 orders of magnitude before it starts to saturate below 4 K. This point corresponds to the transition from the bulk-dominated to surface-dominated regime in which other methods like inverted resistance measurements are needed to separate the bulk and surface resistivities [38]. This method yields at low T a mysterious high-bulk-resistivity plateau, which possibly arises from extended defect conduction [38].

The value of the saturation resistivity at low T, mostly brought by the topological surface states, increases with doping. A possible explanation for this increase is that the disruption of the hybridization by the vacancies introduces a partial smearing of the hybridization gap of the bulk. As a consequence, the surface states acquire a linewidth, and the spin-momentum locking weakens, although the existence of the states still appears to be protected [52,53]. This would allow a certain degree of resistive scattering, which grows with x.

Figure 3 shows the temperature variation of the Hall coefficient R_H in Sm_xB_6 single crystals assuming three-dimensional transport. At high T, R_H reveals activated behavior in all samples in the temperature range 5 K $\lesssim T \lesssim$ 50 K. The activation energy depends on the temperature range, which is consistent with previous Hall resistivity measurements for SmB_6 [1,54,55]. For 15 K $\lesssim T \lesssim$ 50 K, we find $E_A \approx 11$ meV, and for 5 K $\lesssim T \lesssim$ 13 K, $E_A \approx 3.4$ meV. The latter is quite close to the value of the transport gap obtained from the bulk resistivity data. Similar values for the energy gap have been reported from spectroscopy and tunneling experiments [12,17,56–60]. Note that for stoichiometric SmB_6 the resistivity also presents two activation energies separated by a kink around 20 K, the temperature where the in-gap exciton states

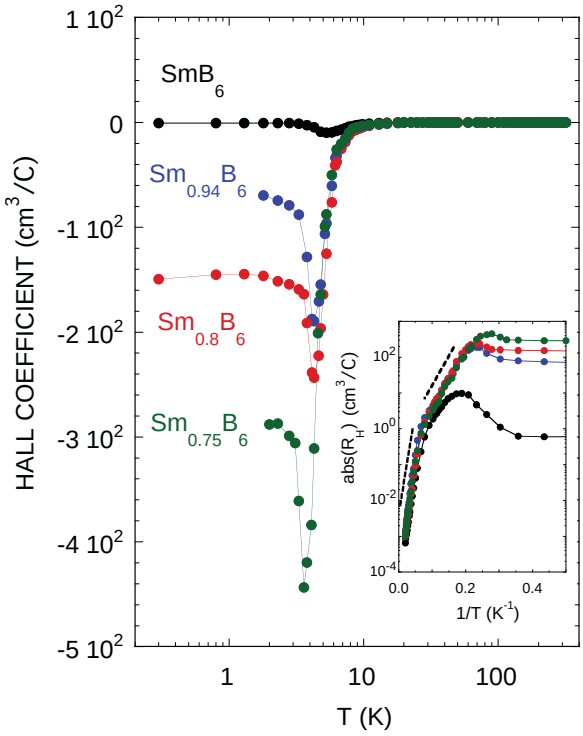

FIG. 3. Hall coefficient R_H vs T for Sm_xB_6 single crystals. In the inset we plot the absolute value of R_H vs $1/T$ for the same samples. The dashed lines show $|R_H| \propto \exp(E_A/k_BT)$ variation.

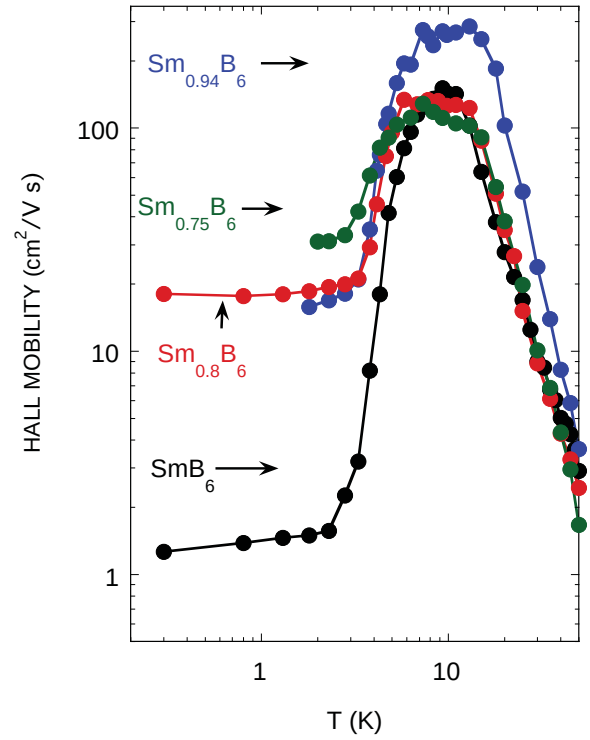

FIG. 4. Hall mobility vs T for Sm_xB_6 single crystals.

emerge. Again, as for R_H, the activation energy for lower T is smaller than the one for higher T [54,61–63].

The measured Hall effect saturates below approximately 3 K, even though the resistivity in this region is still slowly rising in our samples. Electron localization at the Fermi level, brought about by scattering off disordered Sm vacancies [32], could be responsible for such behavior. The low-temperature conductivity proceeds then through hopping. This is consistent with a decrease of the low-temperature conductivity with an increased number of vacancies, as observed. However, the low-temperature Hall mobility, displayed in Fig. 4, shows values which are too high for hopping-activated conduction. The mobility was obtained assuming carriers in a single band, which is justified for sufficiently large x. A two-channel (bulk and surface) conduction model, in which the bulk carrier density decreases exponentially with temperature [10], could be used, but it is difficult to quantify the surface carrier density and mobility at this stage. There is also the possibility of in-gap states participating in electrical conduction. A significant three-dimensional conduction at finite frequencies, originating within the Kondo gap, was recently reported in the insulating bulk of SmB_6 [29]. This contribution is many orders of magnitude larger than any known impurity band conduction. Therefore, it is quite feasible that there is a residual bulk conduction in the Sm_xB_6 system after the surface states set in.

Remarkably, neither the energy gap of Sm_xB_6 crystals seen in the Hall effect nor the transport gap obtained from the resistivity data is affected by disorder brought about by vacancies. These observations apparently contradict recent Raman scattering results showing that Sm vacancies of only 1% can effectively close the gap [39]. However, Raman and dc transport measurements differ significantly in their sensitivity to the band structure. On the other hand, it was found by photoelectron spectroscopy that the intrinsic gap coming from hybridization between *4f* and *5d* states is robust against substitution of Sm for Eu in $Sm_{1-x}Eu_xB_6$ crystals up to $x < 0.5$ [64]. Our results are in line with these findings.

We turn now to the high-temperature Hall effect. R_H changes sign from negative to positive for $T \gtrsim 50$ K in all Sm_xB_6 samples studied. We find that the positive Hall effect roughly follows temperature-dependent paramagnetic susceptibility in the 180 K $\lesssim T \lesssim$ 350 K range. In this region, localized spins on Sm ions are only weakly coupled to the *d* conduction electrons. We expect carrier density not to vary with temperature, but the anomalous skew scattering may considerably affect the Hall coefficient therein. As the temperature is lowered, correlations between localized *f* electrons and conduction electrons are growing stronger. The ordinary contribution to the Hall effect is no longer constant and starts to dominate for $T \lesssim 100$ K.

The Hall effect for mixed-valence compounds is usually written as the sum of a normal (ordinary) contribution, $R_o(T)$, related to the band structure, and an anomalous contribution arising from skew scattering of the conduction electrons off the orbital *f* moment, $R_s(T) = C\rho(T)\chi(T)$, with C being a constant and χ being the susceptibility [65]: $R_H(T) = R_o(T) + R_s(T) = R_o(T) + C\rho(T)\chi(T)$. We use this relation to interpret our data. A plot of R_H versus $\rho\chi$ for Sm_xB_6 samples, shown in Fig. 5, indeed exhibits linear behavior in the temperature range 180 K $\lesssim T \lesssim$ 350 K. This implies

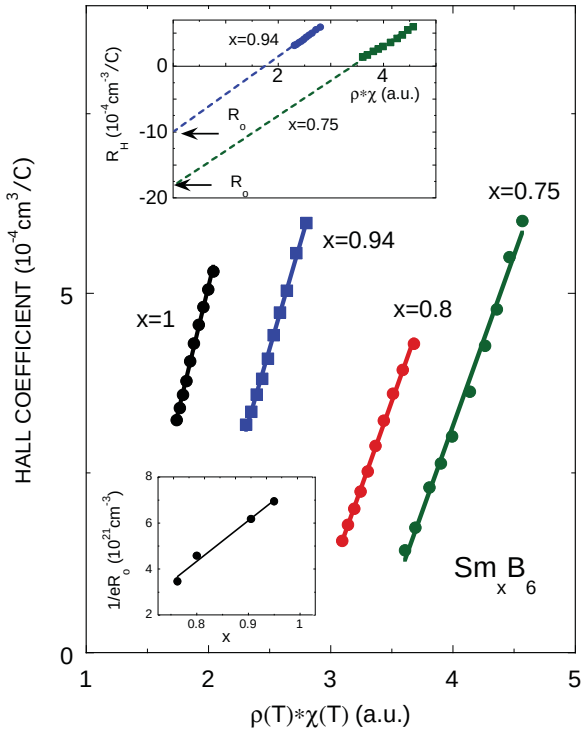

FIG. 5. Hall coefficient vs $\rho\chi$ for Sm_xB_6 single crystals in the $180 \lesssim T \lesssim 350$ K temperature range. In the lower inset we plot the electron concentration values ($=1/eR_o$) as a function of x. The upper inset shows the determination of R_o for the $x = 0.94$ and $x = 0.75$ samples.

that both Hall coefficients (ordinary and anomalous) are independent of T in this region. The ordinate intercept ($=R_o$, see the upper inset in Fig. 5) yields negative values for all samples. The calculated electron concentrations ($=1/eR_o$), using the one-band approximation, are plotted in the lower inset of Fig. 5 vs x. They vary linearly with the number of vacancies in the Sm_xB_6 crystals. Cubic SmB_6 has one Sm ion per unit cell with a valence of about 2.6, and the Sm atom density is 1.42×10^{22} cm^{-3}. This would give rise to an approximate density of 9×10^{21} electrons/cm^3 taking into account that the boron network requires two electrons to form a closed-shell configuration. Our calculated number for $x = 1$ is 7×10^{21} cm^{-3}, close to the expected value.

Next, we examine the heat capacity results. The behavior of the specific heat C_p is the same for all Sm_xB_6 samples, similar to the magnetic and electrical transport properties. Figure 6 shows the molar heat capacity, divided by T, for $T \leqslant 50$ K. Below approximately 10 K, C_p/T shows the typical almost flat behavior, as observed earlier for SmB_6 [28]. The large anomaly, centered at about 35 K in all samples, does not depend on the applied magnetic field, as shown for the $x = 0.94$ sample in the inset of Fig. 6. This feature arises from the hybridization of the $4f$ states in the density of states. It decreases with decreasing x but is not proportional to x since it also contains the phonon contribution [14].

The heat capacity below 10 K, plotted in Fig. 7, shows a particularly rich field and temperature dependence for both the stoichiometric and nonstoichiometric compounds. The

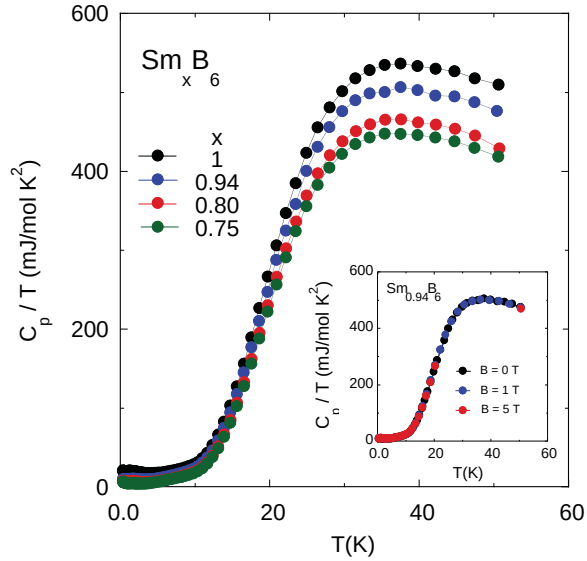

FIG. 6. C_p/T vs T for Sm_xB_6 single crystals. The inset shows C_p/T vs T for the $x = 0.94$ sample at three different magnetic fields.

linear-in-T contribution, $C_{el} = \gamma T$, is predominant, as can be judged from the rather flat behavior of C_p/T in this region. In addition, a Schottky-like anomaly between 1 and 4 K (centered at about 1.5 K) is clearly visible for all samples except the $Sm_{0.75}B_6$ one, and an increase of C_p/T for $T \lesssim 0.8$ K is observed. Because of all these concomitant contributions, it is difficult to determine precisely the electronic specific heat coefficient γ for each sample. As a rough estimation, we assume that γ cannot be larger than the ordinate values corresponding to the dashed lines drawn in Fig. 7. We plot these values vs x in the inset of Fig. 7. It appears that γ increases significantly upon increasing the order of the structure,

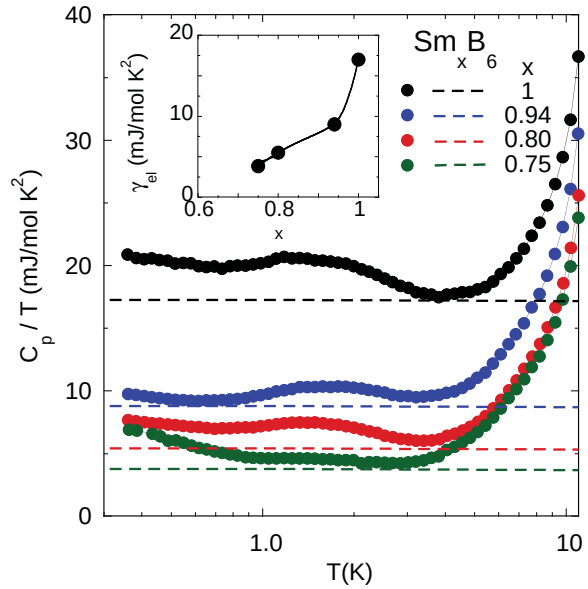

FIG. 7. Low-temperature C_p/T vs T for Sm_xB_6 single crystals. The inset shows the electronic specific heat coefficient vs x.

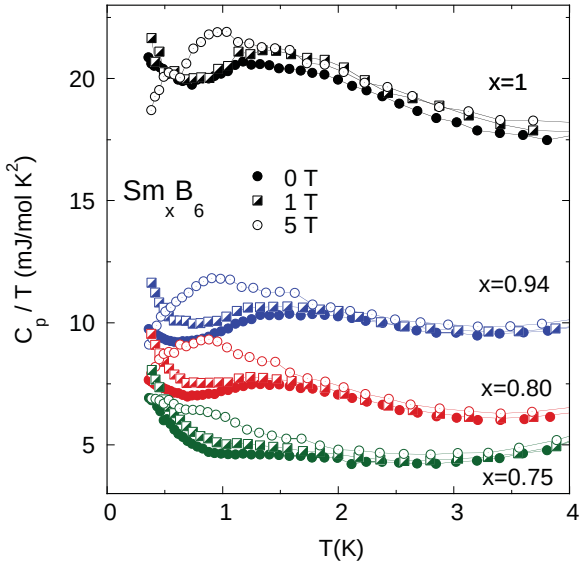

FIG. 8. Low-temperature C_p/T vs T for Sm_xB_6 single crystals at various magnetic fields.

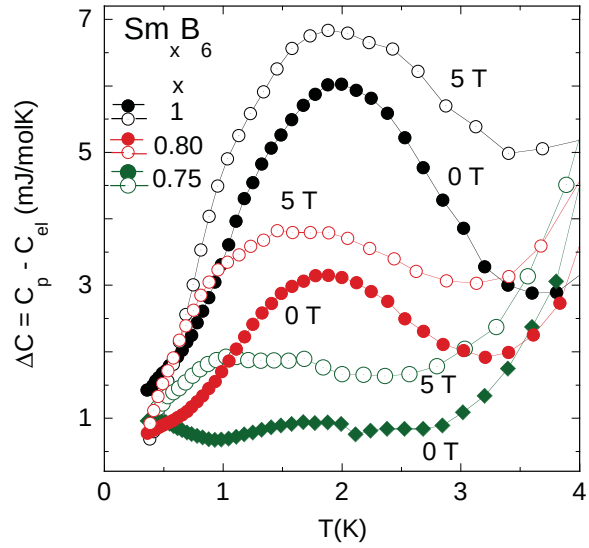

FIG. 9. Low-temperature excess heat capacity $\Delta C = C_p - C_{el}$ for Sm_xB_6 single crystals in various magnetic fields.

reaching the remarkably large value of about 17 mJ/mol K^2 for stoichiometric SmB_6.

The reported values for the electronic specific heat coefficient in SmB_6 span a quite large interval from 1 to 25 mJ/mol K^2 [14,34]. The temperature dependences of C_p/T and the values of γ can vary between samples, but what is puzzling is the origin of this contribution. A low-temperature linear-in-T term is not expected in the specific heat for an insulator and would be negligible for a thin conductive surface. However, it is always seen in SmB_6 and has been shown to be a bulk property [28]. This questions the nature of the low-temperature metal-like properties of SmB_6. Our results are in line with previous results. In addition, we find that the existence of a linear contribution to C_p is robust against vacancy doping.

Figure 8 shows the variation of C_p/T with the applied magnetic field B for all samples studied. The Schottky-like anomaly, centered at about 1.5 K, depends only weakly on B. The lower-temperature rise, which could be attributed to hyperfine interactions, seems to move towards higher T on increasing B. As already noted, $Sm_{0.75}B_6$ is the only composition that does not show clearly the Schottky-like anomaly at 1.5 K, yet it shows the same field-dependent feature at lower temperatures. The ground state of Sm^{3+} has the cubic Γ_8 symmetry [66]. With a very small tetragonal or trigonal distortion of the cube the Γ_8 quartet would split into two doublets. One could speculate that such a splitting could be the origin of a Schottky-like anomaly with weak field dependence.

Finally, we plot the excess heat capacity, $\Delta C = C_p - C_{el}$, which is obtained by subtracting the estimated C_{el} from C_p in Fig. 9. It is clear that the maximum of ΔC at about 2 K becomes smaller as the content of vacancies in Sm_xB_6 gets larger. For $x = 0.75$, this anomaly is hardly seen. The application of a magnetic field has a minor effect on the excess heat capacity.

IV. CONCLUSIONS

As shown by our studies, the overall behavior of the electrical transport, magnetic properties, and heat capacity is qualitatively the same in stoichiometric and nonstoichiometric SmB_6 single crystals. This means that the correlated, possibly topologically nontrivial, state of SmB_6 is only slightly affected by disorder brought about by vacancy doping.

We found that the surface states in Sm_xB_6 are less conductive for $x < 1$, likely as a consequence of impurity scattering in the bulk. The surface states arise from the topological property of the bulk in TIs. Impurities broaden the bulk states, like in any other solid. Since the surface states connect between the valence and conduction bands of the bulk, the linewidth in the bulk is transmitted into the surface states. Although the bulk becomes metallic at low T for lower x, as shown in Ref. [38] with Corbino disk measurements, the existence of surface states appears not to be affected. Moderate disorder does, in general, not change the main topological Z_2 invariants, as observed in Bi alloys [67]. Hence, the insulator stays topological if without disorder it was topological. The other Z_2 invariants may, however, change with disorder. The linewidth of the topological surface states is then associated with small-angle forward scattering but not with backscattering. One could speculate that the topological protection is still in place. In fact, the resistivity plateaus displayed in Fig. 2 occur at higher temperatures and show smaller saturation values when compared to the bulk plateaus in Ref. [38]. Our results deviate somewhat from the Corbino-geometry resistivity measurements for vacancy-doped SmB_6 [38], possibly due to Al contamination in the $x = 1$ sample and an inaccurate bulk resistivity estimation in the low-T surface-dominated regime. Nevertheless, the observed trend is similar, showing that the physical mechanism behind observed electrical transport behavior seems to be unaffected by substantially less samarium in Sm_xB_6 single crystals.

We also found experimentally that the anomalous Hall effect, a characteristic feature of mixed-valent and Kondo

systems [68], is most likely responsible for the change in the Hall coefficient sign for $T \gtrsim 50$ K. As the temperature is lowered, strong electron correlations lead to hybridization of $4f$ states with the itinerant electrons, and the energy gap opens at the Fermi level. The carrier concentration decreases, and the ordinary contribution to the Hall effect becomes dominant, masking the anomalous contribution.

Our low-temperature electron transport results showed some features related to bulk conductivity, possibly through in-gap states. Additionally, heat capacity measurements revealed a very large low-temperature fermionic heat capacity with a γ coefficient that is 17 mJ/mol K^2 in SmB_6. It becomes smaller with increasing doping but is observed up to $x = 0.75$. This contribution seems to be of bulk origin as well. Together, all these observations imply that SmB_6 may not be a perfect topological insulator and both topological surface states and metallic bulk states could be simultaneously present at low temperatures.

ACKNOWLEDGMENTS

We acknowledge support from Grants No. MAT2015-73914-JIN and No. MAT2015-68204-R from the Ministerio de Economía y Competividad of Spain. P.F.S.R. acknowledges support from the DOE/BES Science of 100 Tesla project.

[1] J. W. Allen, B. Batlogg, and P. Wachter, Phys. Rev. B **20**, 4807 (1979).
[2] R. M. Martin and J. W. Allen, J. Appl. Phys. **50**, 7561 (1979).
[3] G. Aeppli and Z. Fisk, Comments Condens. Matter Phys. **16**, 155 (1992).
[4] P. S. Riseborough, Adv. Phys. **49**, 257 (2000).
[5] M. Dzero, K. Sun, V. Galitski, and P. Coleman, Phys. Rev. Lett. **104**, 106408 (2010).
[6] T. Takimoto, J. Phys. Soc. Jpn. **80**, 123710 (2011).
[7] M. Dzero, K. Sun, P. Coleman, and V. Galitski, Phys. Rev. B **85**, 045130 (2012).
[8] V. Alexandrov, M. Dzero, and P. Coleman, Phys. Rev. Lett. **111**, 226403 (2013).
[9] N. Xu, X. Shi, P. K. Biswas, C. E. Matt, R. S. Dhaka, Y. Huang, N. C. Plumb, M. Radović, J. H. Dil, E. Pomjakushina *et al.*, Phys. Rev. B **88**, 121102 (2013).
[10] D. J. Kim, S. Thomas, T. Grant, J. Botimer, Z. Fisk, and J. Xia, Sci. Rep. **3**, 3150 (2013).
[11] M. M. Yee, Y. He, A. Soumyanarayanan, D.-J. Kim, Z. Fisk, and J. E. Hoffman, arXiv:1308.1085.
[12] X. Zhang, N. P. Butch, P. Syers, S. Ziemak, R. L. Greene, and J. Paglione, Phys. Rev. X **3**, 011011 (2013).
[13] S. Wolgast, C. Kurdak, K. Sun, J. W. Allen, D.-J. Kim, and Z. Fisk, Phys. Rev. B **88**, 180405 (2013).
[14] W. A. Phelan, S. M. Koohpayeh, P. Cottingham, J. W. Freeland, J. C. Leiner, C. L. Broholm, and T. M. McQueen, Phys. Rev. X **4**, 031012 (2014).
[15] Y. Luo, H. Chen, J. Dai, Z.-A. Xu, and J. D. Thompson, Phys. Rev. B **91**, 075130 (2015).
[16] M. Neupane, N. Alidoust, S. Xu, T. Kondo, Y. Ishida, D.-J. Kim, C. Liu, I. Belopolski, Y. Jo, T.-R. Chang *et al.*, Nat. Commun. **4**, 2991 (2013).
[17] J. Jiang, S. Li, T. Zhang, Z. Sun, F. Chen, Z. Ye, M. Xu, Q. Ge, S. Tan, X. Niu *et al.*, Nat. Commun. **4**, 3010 (2013).
[18] J. D. Denlinger, J. W. Allen, J.-S. Kang, K. Sun, B.-I. Min, D.-J. Kim, and Z. Fisk, JPS Conf. Proc. **3**, 017038 (2014).
[19] N. Xu, C. Matt, E. Pomjakushina, X. Shi, R. Dhaka, N. Plumb, M. Radović, P. Biswas, D. Evtushinsky, V. Zabolotnyi *et al.*, Phys. Rev. B **90**, 085148 (2014).
[20] W. K. Park, L. Sun, A. Noddings, D.-J. Kim, Z. Fisk, and L. H. Greene, Proc. Natl. Acad. Sci. USA **113**, 6599 (2016).
[21] L. Sun, D.-J. Kim, Z. Fisk, and W. K. Park, Phys. Rev. B **95**, 195129 (2017).
[22] S. Rößler, T.-H. Jang, D.-J. Kim, L. H. Tjeng, Z. Fisk, F. Steglich, and S. Wirth, Proc. Natl. Acad. Sci. USA **111**, 4798 (2014).
[23] T. Miyamachi, S. Suga, M. Ellguth, C. Tusche, C. M. Schneider, F. Iga, and F. Komori, Sci. Rep. **7**, 12837 (2017).
[24] W. Fuhrman, J. Leiner, P. Nikolić, G. E. Granroth, M. B. Stone, M. D. Lumsden, L. DeBeer-Schmitt, P. A. Alekseev, J.-M. Mignot, S. Koohpayeh *et al.*, Phys. Rev. Lett. **114**, 036401 (2015).
[25] N. Wakeham, Y. Q. Wang, Z. Fisk, F. Ronning, and J. D. Thompson, Phys. Rev. B **91**, 085107 (2015).
[26] S. Wolgast, Y. S. Eo, T. Öztürk, G. Li, Z. Xiang, C. Tinsman, T. Asaba, B. Lawson, F. Yu, J. W. Allen *et al.*, Phys. Rev. B **92**, 115110 (2015).
[27] Y. S. Eo, K. Sun, Ç. Kurdak, D.-J. Kim, and Z. Fisk, Phys. Rev. Appl. **9**, 044006 (2018).
[28] N. Wakeham, P. F. S. Rosa, Y. Q. Wang, M. Kang, Z. Fisk, F. Ronning, and J. D. Thompson, Phys. Rev. B **94**, 035127 (2016).
[29] N. J. Laurita, C. M. Morris, S. M. Koohpayeh, P. F. S. Rosa, W. A. Phelan, Z. Fisk, T. M. McQueen, and N. P. Armitage, Phys. Rev. B **94**, 165154 (2016).
[30] T. Caldwell, A. P. Reyes, W. G. Moulton, P. L. Kuhns, M. J. R. Hoch, P. Schlottmann, and Z. Fisk, Phys. Rev. B **75**, 075106 (2007).
[31] B. S. Tan, Y.-T. Hsu, B. Zeng, M. Ciomaga Hatnean, N. Harrison, Z. Zhu, M. Hartstein, M. Kiourlappou, A. Srivastava, M. D. Johannes *et al.*, Science **349**, 287 (2015).
[32] T. Kasuya, K. Takegahara, T. Fujita, T. Tanaka, and E. Bannai, J. Phys. Colloq. **40**, C5-308 (1979).
[33] S. Gabáni, M. Orendáč, G. Pristáš, E. Gažo, P. Diko, S. Piovarči, V. Glushkov, N. Sluchanko, A. Levchenko, N. Shitsevalova, and K. Flachbart, Philos. Mag. **96**, 3274 (2016).
[34] Mat. Orendáč, S. Gabáni, G. Pristáš, E. Gažo, P. Diko, P. Farkašovský, A. Levchenko, N. Shitsevalova, and K. Flachbart, Phys. Rev. B **96**, 115101 (2017).
[35] W. A. Phelan, S. M. Koohpayeh, P. Cottingham, J. A. Tutmaher, J. C. Leiner, M. D. Lumsden, C. M. Lavelle, X. P. Wang, C. Hoffmann, M. A. Siegler *et al.*, Sci. Rep. **6**, 20860 (2016).

[36] G. Pristáš, S. Gabáni, K. Flachbart, V. Filipov, and N. Shitsevalova, JPS Conf. Proc. **3**, 012021 (2014).
[37] T. Kasuya, K. Kojiha, and M. Kasaya, in *Valence Instabilities and Related Narrow-Band Phenomena*, edited by D. Parks (Plenum, New York, 1977).
[38] Y. Eo, A. Rakoski, J. Lucien, D. Mihaliov, Ç. Kurdak, P. S. F. Rosa, D.-J. Kim, and Z. Fisk, arXiv:1803.00959.
[39] M. E. Valentine, S. Koohpayeh, W. A. Phelan, T. M. McQueen, P. F. S. Rosa, Z. Fisk, and N. Drichko, Phys. Rev. B **94**, 075102 (2016).
[40] See Supplemental Material at http://link.aps.org/supplemental/10.1103/PhysRevB.99.045138 for the data on composition, structural characterization, and the surface preparation's role in the transport properties of Sm_xB_6 samples.
[41] P. Wachter, in *Handbook on the Physics and Chemistry of Rare Earths*, edited by K. A. Gschneidner, Jr. and LeRoy Eyring (Elsevier, Amsterdam, 1994), Vol. 19, p. 177.
[42] J. Roman, V. Pavlík, K. Flachbart, Th. Herrmannsdörfer, S. Rehmann, E. S. Konovalova, and Yu. B. Paderno, Phys. B (Amsterdam, Neth.) **230-232**, 715 (1997).
[43] T. Kasuya, J. Phys. Soc Jpn. **65**, 2548 (1996).
[44] P. S. Riseborough, Phys. Rev. B **68**, 235213 (2003).
[45] P. S. Riseborough, Ann. Phys. (Berlin, Ger.) **9**, 813 (2000).
[46] W. T. Fuhrman and P. Nikolić, Phys. Rev. B **90**, 195144 (2014).
[47] P. A. Alekseev, J. M. Mignot, J. Rossat-Mignod, V. N. Lazukov, and I. P. Sadikov, Phys. B (Amsterdam, Neth.) **186-188**, 384 (1993).
[48] V. V. Glushkov, A. V. Kuznetsov, O. A. Churkin, S. V. Demishev, Yu. B. Paderno, N. Yu. Shitsevalova, and N. E. Sluchanko, Phys. B (Amsterdam, Neth.) **378-380**, 614 (2006).
[49] P. Schlottmann, Philos. Mag. **96**, 3250 (2016).
[50] P. Nyhus, S. L. Cooper, Z. Fisk, and J. Sarrao, Phys. Rev. B **55**, 12488 (1997).
[51] Q. Wu and L. Sun, Rep. Prog. Phys. **80**, 112501 (2017).
[52] P. Schlottmann, Phys. Rev. B **90**, 165127 (2014).
[53] N. M. R. Peres, F. Guinea, and A. H. Castro Neto, Phys. Rev. B **73**, 125411 (2006).
[54] N. E. Sluchanko, V. V. Glushkov, S. V. Demishev, A. A. Pronin, A. A. Volkov, M. V. Kondrin, A. K. Savchenko, and S. Kunii, Phys. Rev. B **64**, 153103 (2001).
[55] S. Yeo, K. Song, N. Hur, Z. Fisk, and P. Schlottmann, Phys. Rev. B **85**, 115125 (2012).
[56] K. Flachbart, K. Gloos, E. Konovalova, Y. Paderno, M. Reiffers, P. Samuely, and P. Švec, Phys. Rev. B **64**, 085104 (2001).
[57] B. Gorshunov, N. Sluchanko, A. Volkov, M. Dressel, G. Knebel, A. Loidl, and S. Kunii, Phys. Rev. B **59**, 1808 (1999).
[58] H. Ohta, R. Tanaka, M. Motokawa, S. Kunii, and T. Kasuya, J. Phys. Soc. Jpn. **60**, 1361 (1991).
[59] T. Nanba, H. Ohta, M. Motokawa, S. Kimura, S. Kunii, and T. Kasuya, Phys. B (Amsterdam, Neth.) **186-188**, 440 (1993).
[60] G. Travaglini and P. Wachter, Phys. Rev. B **29**, 893 (1984).
[61] D. J. Kim, J. Xia, and Z. Fisk, Nat. Mater. **13**, 466 (2014).
[62] N. E. Sluchanko, A. A. Volkov, V. V. Glushkov, B. P. Goshunov, S. V. Demishev, M. V. Kondrin, A. A. Pronin, N. A. Samarin, Y. Bruynseraede, and S. Kunii, JETP **88**, 533 (1999);
[63] F. Chen, C. Shang, Z. Jin, D. Zhao, Y. P. Wu, Z. J. Xiang, Z. C. Xia, A. F. Wang, X. G. Luo, T. Wu, and Z. H. Chen, Phys. Rev. B **91**, 205133 (2015).
[64] J. Yamaguchi, A. Sekiyama, M. Y. Kimura, H. Sugiyama, Y. Tomida, G. Funabashi, S. Komori, T. Balashov, W. Wulfhekel, T. Ito *et al.*, New J. Phys. **15**, 043042 (2013).
[65] A. Fert and P. M. Levy, Phys. Rev. B **36**, 1907 (1987).
[66] M. Sundermann, H. Yavaş, K. Chen, D.-J. Kim, Z. Fisk, D. Kasinathan, M. W. Haverkort, P. Thalmeier, A. Severing, and L. H. Tjeng, Phys. Rev. Lett. **120**, 016402 (2018).
[67] M. Z. Hasan and C. L. Kane, Rev. Mod. Phys. **82**, 3045 (2010).
[68] P. Coleman, P. W. Anderson, and T. V. Ramakrishnan, Phys. Rev. Lett. **55**, 414 (1985).